MIST Topology Optimization for Bending Plates under Static Loading

Mahmoud Alfouneh[1], Liyong Tong[2]

[1] School of Aerospace, Mechanical and Mechatronic Engineering, The University of Sydney, NSW, Australia, Mahmoud.alfouneh@usyd.edu.au
[2] School of Aerospace, Mechanical and Mechatronic Engineering, The University of Sydney, NSW, Australia, liyong.tong@usyd.edu.au

Abstract
This article extends the moving iso-surface threshold (MIST) method to solve the topology optimization problem of bending plates under static loading. In the extended MIST, multiple layer-wise objective functions and volume constraints are employed in the optimization formulation of multiple-layered bending plates. Considered are three types of objective functions: minimum mean compliance, maximum mutual strain energy and fully-stressed design. The associated response functions chosen are, respectively, the strain energy density, mutual strain energy density and the Von Mises stress for each layer. The nodal values of these response functions in a fixed FE mesh are smoothed using a modified filter. Numerical examples are presented to validate the extended MIST in application to topology optimizations of single- and multi-layered plates under static loading.

Keywords: MIST topology optimization, multi-layer plate, minimum mean compliance, compliance mechanism, fully-stressed design.

1. Introduction

Topology optimization of bending plates is about finding the optimum material distribution to achieve optimum or better performance. Bending plates can come in the form of a single-layer or multiple-layers and its topology optimization is conducted for one or multiple layers. Topology optimization of bending plates and shells under static loading has attempted by a number of researchers using different optimization methods [1-10]. In this study, we extend the MIST method [11-12] to the case of topology optimization with multiple layer-wise objective functions and volume constraints. MIST method has applied for solving some 2D plane stress or strain or 3D problems, but has not been used to study the topology optimization of bending plates, in particular multiple layered plates, under static loading. The article is organized as follows. Section 2 presents the problem statement with multiple layer-wise objective functions and volume constraints. Section 3 presents some implementation details of the MIST method. Section 4 presents several numerical examples including single-layered or multiple-layered bending plates under static loadings. A brief summary is provided in Section 5.

2. Problem statement

For a single- or multiple layered bending plates under static loading, we define its topology optimization problem as follows:

$$
\begin{aligned}
&\min or \max f_i \quad (i=1,2,...n) \\
&\text{subject to:} \quad \mathbf{K}\mathbf{U}_{(j)} = \mathbf{F}_{(j)} \quad (j=1,2) \\
&\qquad\qquad \sum_{k=1}^{N_E}(x_{ki}A_k) = \alpha_i \sum_{k=1}^{N_E}A_k \qquad (\varepsilon \le x_{ki} \le 1; \quad i=1,2,...,n)
\end{aligned}
\tag{1}
$$

where f_i and α_i are the objective function and the material volume fraction for the ith layer, n is the total number of layers in a multiple-layered plate, $\mathbf{K}$ is the global stiffness matrix of the plate structure, $\mathbf{U}_j$ and $\mathbf{F}_j$ are the nodal displacement and load vectors for the jth load case (where j=1 refers to the real load case, whereas j=2 represents the dummy load case with an applied unit load at chosen degree of freedom, x_{ki} is the weighting factor or density of the kth element for the ith layer and varies from 0 to 1 ($x_{ki}=0$ means void and $x_{ki}=1$ indicates solid), A_k is the volume or area of the kth element, and N_E represents the total number of elements for each layer (In this study same N_E is used for the numerical examples). In the literature, $\varepsilon = 0.001$ is typically chosen in numerical computations to avoid stiffness matrix singularity.

Three types of objective functions are considered in this study and the corresponding statements are:

(a) to minimize the mean compliance i.e.

$$\min f_i = \int_{\Omega_i} \tfrac{1}{2}\boldsymbol{\sigma}_i^T \boldsymbol{\varepsilon}_i d\Omega \tag{2a}$$

(b) to maximize the deflection in the direction of a chosen degree of freedom, i.e.

$$\max f_i = u_{out} = \int_{\Omega} \boldsymbol{\sigma}_{(2)}^T \boldsymbol{\varepsilon}_{(1)} d\Omega, \text{ or } \min f_i = -u_{out} = -\int_{\Omega} \boldsymbol{\sigma}_{(2)}^T \boldsymbol{\varepsilon}_{(1)} d\Omega \tag{2b}$$

and

(c) to minimize the maximum Von Mises stress, i.e.

$$\min f_i = \sum_{k=1}^{Nnode} \sigma_{vmk}^{(i)} \tag{2c}$$

Where $\sigma_{vmk}^{(i)}$ denotes the Von Mises stress at the kth node for the ith layer and N_{node} denotes the total number of nodes for each layer.

3. MIST algorithm and implementation

The MIST algorithm can be schematically depicted in the flowchart in Figure 1.
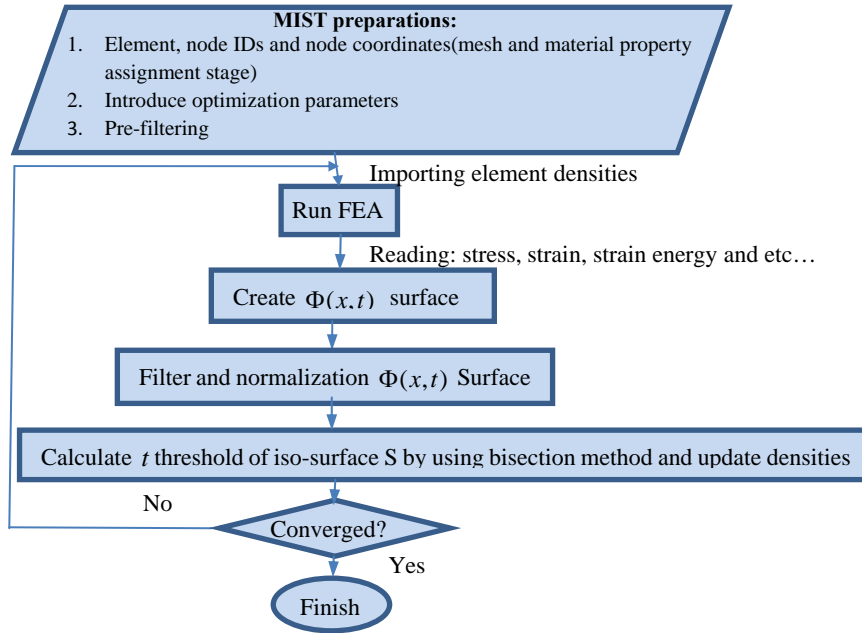

Figure 1: MIST algorithm flowchart

The MIST method is interfaced with ANSYS to solve all the FEM problems. In each iteration after each FEA run, selected FEA results, such as strain energy density, strain and stress are imported from the ANSYS output files and then used to construct the response function Φ for the design domain. For the three types of problems given in equations (1) and (2), the Φ function for the ith iteration is, respectively, given by:

$$\Phi_i(x,t) = \tfrac{1}{2}\boldsymbol{\sigma}_i^T \boldsymbol{\varepsilon}_i \tag{3a}$$

$$\Phi_i(x,t) = -\tfrac{1}{2}\boldsymbol{\sigma}_{i(2)}^T \boldsymbol{\varepsilon}_{i(1)} \tag{3b}$$

$$\Phi_i(x,t) = \sigma_{vmi} \tag{3c}$$

where $\boldsymbol{\varepsilon}_{i(1)}$ and $\boldsymbol{\sigma}_{i(2)}$ represent the strain and stress vectors for load case 1 and 2 respectively. Nodal values of Φ function can be either output from ANSYS or calculated by using relevant stress or strain values at Gaussian or nodal points.

In MIST, a filtering scheme is applied to the nodal values of Φ function. Consider node j, the filtered value of Φ_j, denoted by $\hat{\Phi}_j$, can be determined by

$$\hat{\Phi}_j = \frac{\Phi_{qj}}{c_{uj}} \tag{4a}$$

where

$$c_{uj} = \sum_{q=1}^{N_q} c_{fq} \qquad (4b)$$

$$\Phi_{qj} = \sum_{q=1}^{N_q} c_{fq} \Phi_q \qquad (4c)$$

and

$$c_{fq} = \pi (r_{min} - R_{jq})^2 \qquad (4d)$$

where r_{min} is the spatial radius (typically of the value of approximately 3 times of element length), N_q denotes the number of nodes that lie within the circle with a radius of r_{min}, R_{jq} is the distance between node j and q. Φ_q is the Φ value at node q which lies within the circle.

The elastic modulus of an element in a structure is updated using:

$$E(x_k)_i = (x_k^p)_i \, E_{(solid)_i} \qquad (5)$$

Where x_k represents the fraction of solid area to the total one of the kth element and p is the penalty factor.

4. Numerical results and discussion

4.1 Minimum mean compliance

The problem considered in this section is the minimum mean compliance problem or the problem of minimizing the total strain energy of the structure. Firstly, for single-layer plate, we study the effects of spatial radius and the volume fraction on the selected results of topology design optimization using MIST, e.g. the objective function versus iteration histories and the final topologies; Secondly, we investigate the topology optimization of multiple layers in multi-layered plates. In all the calculations for this problem, the Φ function defined in equation (3a) is adopted. For the case of multiple-layered plates, the Φ function given in equation (3a) is used to construct the relevant response function for every design layer.

4.1.1 Effect of spatial radius r_{min}

Consider the topology optimization of a four-side clamped square plate with side length of 60mm and thickness of 0.5mm subject to a point load F_z=-5N at its centre and a volume fraction of 0.5. Assume E=70000 MPa and v=0.3. The square plate is meshed with 3600 (60 elements by 60 elements) solid181 elements in ANSYS. As in MIST, we use the following parameters: move limit=0.1, penalty factor=3. Figure 2 depicts the curve of the total strain energy versus iteration for r_{min} =7mm. It is evident that the objective function converges rapidly and smoothly.

Figure 3 depicts the final optimum topologies for various values of spatial radius r_{min} e.g., 1, 3, 6 and 7 mm or 1, 3, 6 and 7 element lengths. As shown in Figure 3, for small spatial radius hinges exist in the optimum topologies, whereas for large spatial radius these hinges disappear, which makes the topology more practical in the sense of load diffusion.
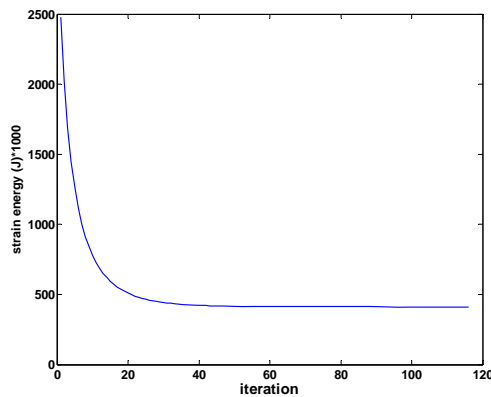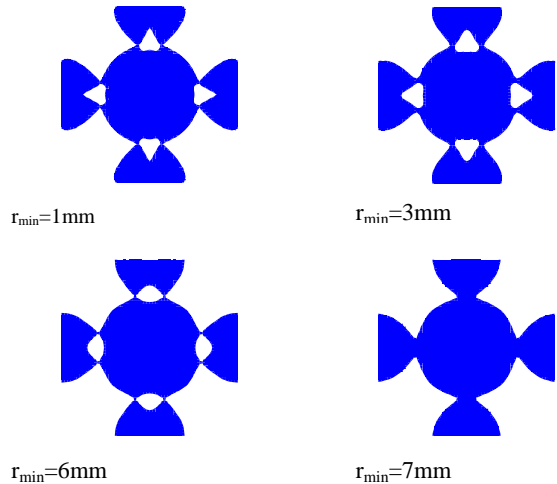

Figure 2: The objective function- iteration history

r_{min}=1mm r_{min}=3mm

r_{min}=6mm r_{min}=7mm

Figure 3: The effects of filtering radius on the optimal topology

4.1.2 Influence of volume fractions

Consider the same plate as used in example 4.1.1 except for the four-side clamped boundary condition being replaced by four-side simply supported one. This example is to illustrate the effect of the volume fraction on the convergence history of the objective function and the final optimum topologies. Figure 4 depicts the curves of the objective function versus iteration number for four different volume fractions, e.g. 20%, 40%, 60% and 80%. It is noted that the objective function converges with 50 iterations for 20% and 40% volume fractions and with 30 for the cases of 60% and 80% volume fractions. Figure 5 depicts the final topologies for the four volume fraction cases. It can be seen that the topologies for the 20% and 40% or the 60% and 80% volume fractions resembles to certain extent, the difference between the topologies for the 20% and 40% volume fractions are quite different from the other two topologies with 60% and 80% volume fractions. There appears a topological shape change when the volume fraction varies from 40% to 60%.
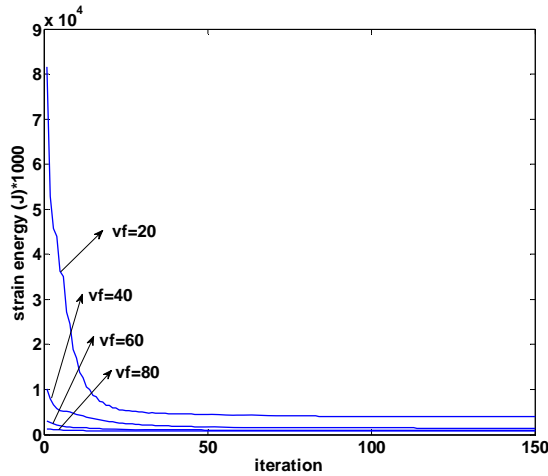

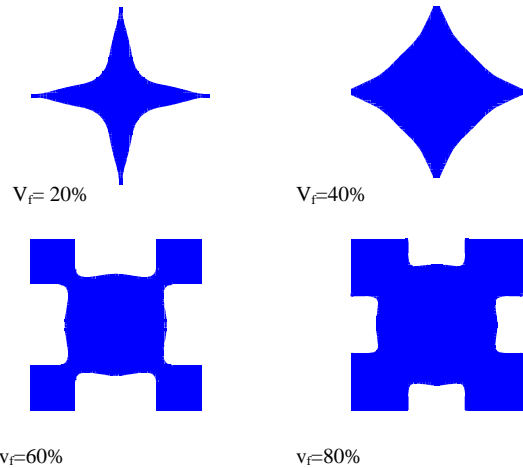Figure 4: Variations of strain energy versus iteration for different v_f

Figure 5: Different optimal shapes with different v_f

4.1.3 Multiple-layered plate

Consider a four-side clamped four-layer square plate. The side length is 300 mm, and the thickness of each layer is 1 mm ($t_1=t_2=t_3=t_4=1mm$). The material properties for all four layers are: $E_1=E_4=69$ GPa, $E_2=E_3=220$ MPa, $v_1=v_3=v_4=0.3$, $v_2=0.49$. At the centre of the square plate a vertical point load $F_z=-200N$ is applied. A total number of 3600 (ANSYS Solid185) elements are used to uniformly mesh each layer. In all the MIST calculations, the following parameters are used: dynamic move limit of minimum=0.1, spatial radius=0.0125mm in filtering, and penalty factor = 3. Layers 2 and 4 are the design layers with $v_{f2} = v_{f4}= 50\%$. Figure 6 depicts the convergence histories of the total strain energies calculated for the second layer, the fourth layer and all layers. Evidently, the total strain energies for the second, fourth and all layers converge within 100 iterations.
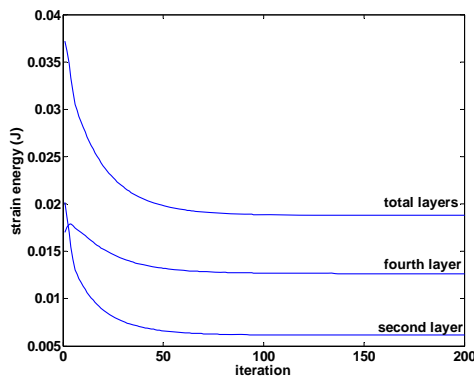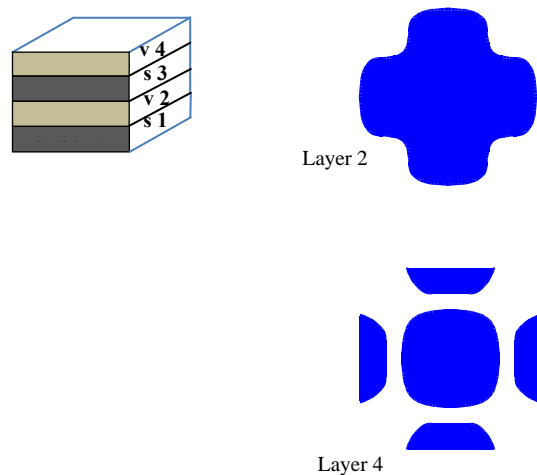

Figure 6:Iteration histories for different layers

Figure 7: Optimum shapes of layers 2 and 4

4

Figure 7 depicts the sketch of the four-layer plate and the optimum topologies of layers 2 and 4. The material distribution of layer 4 is discontinuous whereas that for layer 2 has a continuous load diffusion path with the layer.

4.2 Compliance mechanism

The objective function for this example is to maximize deflection under dummy load based on Φ function introduced in equation (3b).A three layer plate which layer 3 (top layer) is under design layer with volume fraction v_{f3}=50%, is considered. Two other layers are non-design layers (figure 9). The plate dimensions and material properties are the same as example 4.1.3 except at this example there is not layer 4. The elements, meshing scheme and solver used are also the same as example 4.1.3. The plate is clamped at left edge. Two load cases are applied. Load case 1, $FR = -200\,N$ is real load and applied vertically at the centre of plate and load case 2 is dummy load $FU = -1N$ applied in z direction same as direction of real load at the centre of opposite edge.
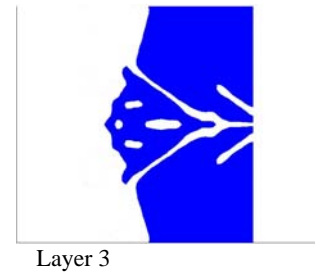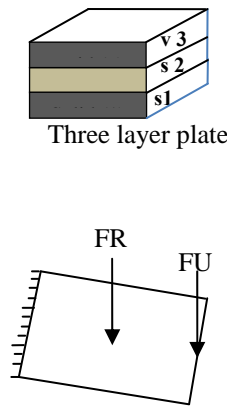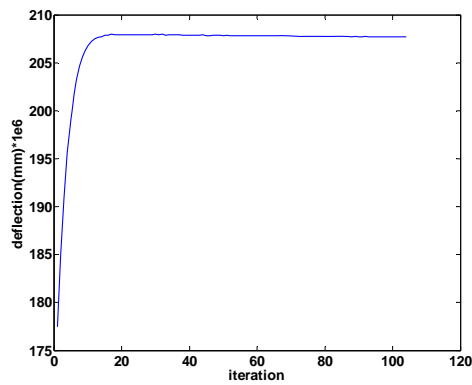

Three layer plate

Layer 3

Figure 8: iteration histories versus deflection under dummy load   Figure 9: optimal shape

As can be seen from figure 8, deflection under dummy load is maximised alongside of optimization increment and finally it is stabled. The initial value for objective function is approximately 177e-6 mm which reaches to a stable value around 207 e-6 mm in just 20 iterations. It is a considerable maximization about 1.169 times of initial value. Small fluctuations as seen in iteration history curve can be removed by considering low values of move limit say lower than 0.1. Corresponding optimal shape is demonstrated in figure 9 and it is shown that material distributed in the right half side of design layer.

4.3 Fully-stressed design

The aim of this example is to use the Φ function given in equation (3c) to develop fully stressed designs for selected layers. The plate is clamped at four sides and a force of Fz=-200 N is applied at the center. The plate dimensions and material properties are the same as example 4.1.3. The elements, meshing scheme and solver used are also the same as example 4.1.3. As shown in Figure 11, the inner two layers are non-design layers whereas the outer two layers are the design layers with different volume factions, e.g. v_{f1}=70% and v_{f4}=20%. Figure 10 shows the iteration histories of the total von Mises stress in layer 1, layer 4 and all layers. Once again, all three quantities converge within 60 iterations. As shown in this figure, minimizing total Von Mises stress happen as expected for all the design layers. It is seen that for layer 4 the reduction happens visibly although these values are so small since its volume fraction is much lower than layer 1. Figure 11 depicts the corresponding topologies of layer 1 and layer 4. It is noted that the topology in layer 4 resembles to that in layer 4 in example 4.1.3 as both layers are in compression in the bending plate.
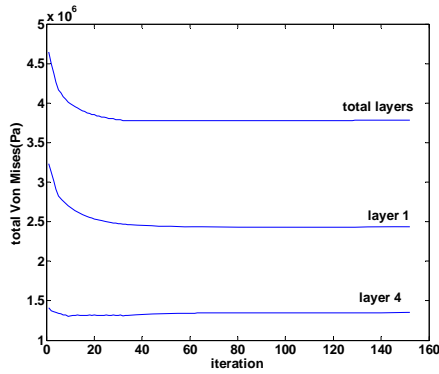
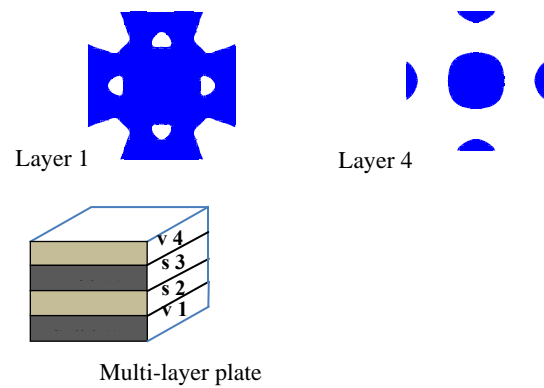Figure 10: Iteration histories for fully stressed design

Figure 11: optimal shapes for top and bottom layers

5. Concluding remarks

The salient points of the present study can be summarized as follows: (a) an extended MIST formulation is presented for topology optimization of multiple-layered plate structures with multiple volume fractions; (b) three problems with different objective functions are considered and then solved by using three different response functions; and (c) the present numerical results illustrate the effects of the spatial radius in the filter used and the volume fraction on the optimum topologies as well as the stable convergence history observed.

Acknowledgements

References

1. Liang, Q.Q., Y.M. Xie, and G.P. Steven, A performance index for topology and shape optimization of plate bending problems with displacement constraints. *Structural and Multidisciplinary Optimization*, 2001. **21**(5): p. 393-399.
2. Zhao, C., G. Steven, and Y. Xie, Evolutionary natural frequency optimization of thin plate bending vibration problems. *Structural optimization*, 1996. **11**(3-4): p. 244-251.
3. Kang, Z. and X. Wang, Topology optimization of bending actuators with multilayer piezoelectric material. *Smart Materials and Structures*, 2010. **19**(7): p. 075018.
4. Belblidia, F., J. Lee, and S. Rechak, Topology optimization of plate structures using a single-or three-layered artificial material model. *Advances in Engineering Software*, 2001. **32**(2): p. 159-168.
5. Mukherjee, A. and S. Joshi, Piezoelectric sensor and actuator spatial design for shape control of piezolaminated plates. *AIAA journal*, 2002. **40**(6): p. 1204-1210.
6. Halkjær, S., O. Sigmund, and J.S. Jensen, Maximizing band gaps in plate structures. *Structural and Multidisciplinary Optimization*, 2006. **32**(4): p. 263-275.
7. Pedersen, N.L., On topology optimization of plates with prestress. *International Journal for Numerical Methods in Engineering*, 2001. **51**(2): p. 225-239.
8. Stegmann, J. and E. Lund, Nonlinear topology optimization of layered shell structures. *Structural and Multidisciplinary Optimization*, 2005. **29**(5): p. 349-360.
9. Kögl, M. and E.C. Silva, Topology optimization of smart structures: design of piezoelectric plate and shell actuators. *Smart materials and Structures*, 2005. **14**(2): p. 387.
10. Hansel, W. and W. Becker, Layerwise adaptive topology optimization of laminate structures. *Engineering Computations*, 1999. **16**(7): p. 841-851.
11. Tong, L. and J. Lin, Structural topology optimization with implicit design variable—optimality and algorithm. *Finite Elements in Analysis and Design*, 2011. **47**(8): p. 922-932.
12. Vasista, S. and L. Tong, Design and testing of pressurized cellular planar morphing structures. *AIAA journal*, 2012. **50**(6): p. 1328-1338.